

Irregular Liesegang-type patterns in gas phase revisited. I. Experimental setup, data processing, and test of the spacing law

José C. Torres-Guzmán, Thomas Buhse, Elsa María de la Calleja, Alfredo González-Espinoza, Gustavo Martínez-Mekler, Fernando Montoya-Nava, Elizeth Ramírez-Álvarez, Marco Rivera-Islas, Aurora Rodríguez-Álvarez, and Markus F. Müller

Citation: [The Journal of Chemical Physics](#) **144**, 174701 (2016);

View online: <https://doi.org/10.1063/1.4946791>

View Table of Contents: <http://aip.scitation.org/toc/jcp/144/17>

Published by the [American Institute of Physics](#)

Articles you may be interested in

[Irregular Liesegang-type patterns in gas phase revisited. II. Statistical correlation analysis](#)

The Journal of Chemical Physics **144**, 174702 (2016); 10.1063/1.4946792

[On the estimation of phase synchronization, spurious synchronization and filtering](#)

Chaos: An Interdisciplinary Journal of Nonlinear Science **26**, 123106 (2016); 10.1063/1.4970522

[Nucleation and colloidal growth in concentration gradients \(Liesegang rings\)](#)

The Journal of Chemical Physics **77**, 1302 (1998); 10.1063/1.443952

[Synchronization using environmental coupling in mercury beating heart oscillators](#)

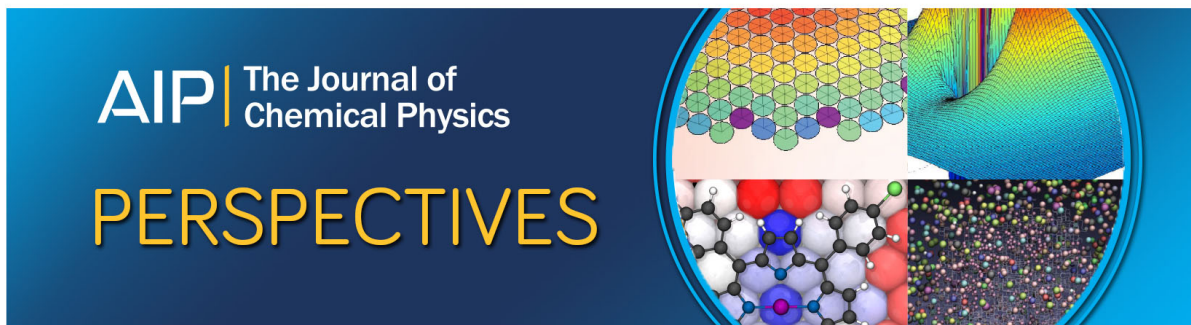
Chaos: An Interdisciplinary Journal of Nonlinear Science **26**, 063103 (2016); 10.1063/1.4953014

[Tracking stochastic resonance curves using an assisted reference model](#)

Chaos: An Interdisciplinary Journal of Nonlinear Science **25**, 063107 (2015); 10.1063/1.4922185

[A new universal law for the Liesegang pattern formation](#)

The Journal of Chemical Physics **122**, 184707 (2005); 10.1063/1.1893606



Irregular Liesegang-type patterns in gas phase revisited. I. Experimental setup, data processing, and test of the spacing law

José C. Torres-Guzmán,¹ Thomas Buhse,² Elsa María de la Calleja,^{3,a)}

Alfredo González-Espinoza,^{3,4} Gustavo Martínez-Mekler,^{3,5,6} Fernando Montoya-Nava,^{4,b)}

Elizeth Ramírez-Álvarez,^{1,c)} Marco Rivera-Islas,¹ Aurora Rodríguez-Álvarez,⁴
and Markus F. Müller^{1,5,6,d)}

¹Centro de Investigación en Ciencias, Universidad Autónoma del Estado de Morelos,
Avenida Universidad 1001, Cuernavaca, Morelos 62209, Mexico

²Centro de Investigaciones Químicas, Universidad Autónoma del Estado de Morelos,
Avenida Universidad 1001, Cuernavaca, Morelos 62209, Mexico

³Instituto de Ciencias Físicas, Universidad Nacional Autónoma de México, Apartado Postal 48-3,
Cuernavaca, Morelos 62251, Mexico

⁴Instituto de Investigación en Ciencias Básicas y Aplicadas, Universidad Autónoma del Estado de Morelos,
Avenida Universidad 1001, Cuernavaca, Morelos 62209, Mexico

⁵Centro Internacional de Ciencias A. C., Avenida Universidad 1001, Cuernavaca, Morelos 62131, Mexico

⁶Centro de Ciencias de la Complejidad, Universidad Nacional Autónoma de México, Ciudad Universitaria,
México, D. F. 04510, Mexico

(Received 17 December 2015; accepted 29 March 2016; published online 2 May 2016)

Since the early work on Liesegang rings in gels, they have been a reference point for the study of pattern formation in chemical physics. Here we present a variant of the Liesegang experiment in gas phase, where ammonia and hydrochloric acid react within a glass tube producing a precipitate, which deposits along the tube wall producing a spatial pattern. With this apparently simple experiment a wide range of rich phenomenon can be observed due to the presence of convective flows and irregular dynamics reminiscent of turbulent behavior, for which precise measurements are scarce. In this first part of our work, we describe in detail the experimental setup, the method of data acquisition, the image processing, and the procedure used to obtain an intensity profile, which is representative of the amount of precipitate deposited at the tube walls. Special attention is devoted to the techniques rendering a data series reliable for statistical studies and model building, which may contribute to a characterization and understanding of the pattern formation phenomenon under consideration. As a first step in this direction, based on our data, we are able to show that the observed band pattern follows, with slight deviations, the spacing law encountered in common Liesegang rings, despite that the experimental conditions are very different. A further statistical correlation analysis of the data constitutes Paper II of this research. Published by AIP Publishing. [<http://dx.doi.org/10.1063/1.4946791>]

I. INTRODUCTION

Liesegang patterns have been widely studied for more than a century.¹ They emerge in nature in many systems as a result of reaction-diffusion-precipitation phenomena. In one of the simplest experimental realizations, a reactant *A* diffuses into a gel that contains a solute *B*. When *A* and *B* encounter, an insoluble product *C* is formed that may diffuse² or not³ to eventually form band or ring structures. Such band or ring formation occurs when the concentration of *C* reaches a threshold value after which nucleation, aggregation, and growth processes initiate.⁴ These processes deplete the

concentration of *A* and *B* in the reaction zone causing concentration gradients that in turn trigger diffusive fluxes. Consequently, the reaction front propagates successively by passing the regions of the last formed bands or rings until the proper condition, i.e., the critical concentration of *C*, for the onset of further precipitation processes is reached elsewhere.

Regular Liesegang patterns are mostly obtained in gel systems, also more complex structures like mosaic pattern,⁵ tree-like crystallization,⁶ wave-like structures and speckled pattern⁷ have been observed. For the Liesegang patterns in gel systems three laws concerning the spatial position *y_n*, the formation time *t_n*, and the width *w_n* of the *n*th band are usually satisfied: time law *y_n ∝ √t_n*,⁸ spacing law *y_{n+1} = p y_n*,⁹ and width law *w_n ∝ y_n^α*.¹⁰ In addition, a law relating the parameter *p* to the initial concentrations of the reactants has been reported.¹¹ In other studies secondary structures or irregular band spacing is described.^{12,13} These particular features, mostly caused by the specific experimental setup such as geometry or physical properties of substrates,

a)Present address: Instituto de Física, Universidade Federal do Rio Grande do Sul, Caixa Postal 15051 - CEP 91501-970 - Porto Alegre, RS, Brazil.

b)Present address: Instituto de Biotecnología, Universidad Nacional Autónoma de México, 62251 Cuernavaca, Morelos, México.

c)Present address: Nonequilibrium Chemical Physics, Physik-Department, TU-München, James-Franck-Str. 1, 85748 Garching bei München, Germany.

d)E-mail: muellerm@uaem.mx

are also observed in the vapor to particle HCl–NH₃ system. Such behavior is difficult to characterize quantitatively in these kind of systems, which is likely to be the reason why the rationalization of Liesegang phenomena was mainly concerned with the derivation of empirical laws based on gel systems in contrast to the here treated vapor-to-particle system.

With regard to numerical simulations, mean-field approximations,¹⁴ automata models¹⁵ as well as reaction-diffusion-systems using the Lattice-Boltzmann method¹⁶ have been proposed to describe the formation of regular patterns in a quantitative manner. For a comparison between theoretical advances and experimental results see Ref. 17. However, up to now no single model can explain all the observed results like the reverse spacing,¹⁸ or the formation of double banding.^{19,20}

A variant of the Liesegang experiment is realized in the gas phase,²¹ where at each end of a long air-filled glass tube a reactant is let to diffuse inwards the recipient.²² The main difference between gas and gel phase is that gel prevents convection, while in gas phase, under proper conditions, the reaction-diffusion system may turn into a reaction-diffusion-convection one. Furthermore, experiments of the gas-phase seem to depend sensitively on changes in temperature or pressure. If small temperature fluctuations are diminished, also fluctuations of the pressure within the tube are minimized. In this case, it was reported that a continuous precipitation occurred instead of the formation of discrete bands.²³

In this work, we study the NH₃–HCl system in gas phase at room temperature. Our main goal is to set up an experiment capable of producing well-defined Liesegang-type bands and to implement image and data pre-processing techniques that produce, with precision and confidence, series amenable for statistical analysis and model building. Most of these statistical studies are carried out in Paper II.³² Here we test solely the spacing law $y_{n+1} = py_n$ for the irregular patterns obtained in the experiment.

We choose a glass tube in upright position with a diameter large enough so that convection processes may occur. Actually, the convection within the reaction zone becomes visible by simple eye inspection of the experiment. The reaction product (NH₄Cl) becomes apparent as a white seemingly turbulent cloud of microscopic salt particles, which produces a multitude of deposition bands in a rather irregular manner while moving along the tube. In a recent work,²⁴ a variety of such experiments was presented and the three-dimensional structure of the reaction cloud was described in detail. Depending on the experimental conditions like the tube-radius and geometry, beautiful turbulences called “micro-tornadoes,” “micro-stalactites,” and “micro-geysers” were observed by using a laser technique, giving rise to seemingly different dynamical formations and different precipitation patterns like rings or spirals.

To the best of our knowledge, a quantitative analysis of this type for Liesegang patterns in the gas phase is still pending. This might be due to the fact that the quantitative determination of both, exact position and intensity of a precipitation band is not a trivial task. Many circumstances obstruct the precise assessment of band positions and

intensities from the precipitation pattern of a glass tube. In the present work we develop a comprehensive procedure of data acquisition and pre-processing before we apply in a forthcoming publication, a variety of different statistical techniques of data analysis. For this purpose, we discuss the different types of error sources and the data pre-processing, necessary to reduce or eliminate a variety of systematic measurement errors and the influence of stochastic noise sources, which influence drastically the formation of band sequences. We assume that the resulting intensity profile, visible on photographs, represents the genuine amount of precipitate deposited on the walls as a function of the position along the tube. Under this assumption, we analyze maxima in the intensity profile and interpret them as bands, in order to check if the spacing law $y_{n+1} = py_n$ is fulfilled, or if there is at least a reminiscence of it imprinted in the sequence of bands.

The paper is structured as follows: In Section II we describe the experimental setup and identify several sources of measurement errors. In Section III we take into account such circumstances and develop a procedure of data acquisition and pre-processing that render a dependable intensity profile. In Section IV we test for the spacing law $y_{n+1} = py_n$, and finally in Section V we give our conclusions.

II. EXPERIMENTAL SETUP

Figure 1(a) shows an image of the experimental setup used in the present study. It consists of a vertically mounted glass tube of 1.22 m length and 3.0 cm inner diameter. The tube is thoroughly cleaned, rinsed with distilled water, and dried prior to each experiment, containing atmospheric air initially. Both ends of the tube are sealed. Small cotton balls are anchored to the interior of each end of the tube and moistened by injection of 0.5 ml aqueous solutions of HCl (36.5%–38.0%, Baker, ACS reagent) at the bottom end and NH₃ (28%–30%, Sigma-Aldrich, ACS reagent) at the top end. Considering the molecular weights of HCl and NH₃ relative to air, this choice favors reactant movement by diffusion. Subsequently, the system evolves at room temperature. Both reactants evaporate from the cotton balls and diffuse along the tube toward each other so that eventually the chemical reaction initiates. Experiments were carried out ensuring a sufficient humidity in the environment since water is thought to be a catalyst in the chemical reaction.²⁵ When we reduced the amount of water we ceased to observe any pattern formation, water is essential for the formation of ammonium chloride. As the reaction front moves towards the bottom of the tube, the reaction product is successively imprinted as irregular bands at the tube wall. A surprising aspect of this exothermic reaction is the notable spatial extension of the reaction cloud. It is reminiscent of a jellyfish moving backwards, with a bell-shaped top and a pronounced tentacle region. Particle deposition at the tube wall occurs at the rim of the bell. Although the cloud dynamics has a strong turbulent-like component, one also observes a kind of pulsating behavior. Eventually, a stream of micro-particles, originating from the tentacle region, pushes its way towards the bell, which in consequence becomes more bent and looses

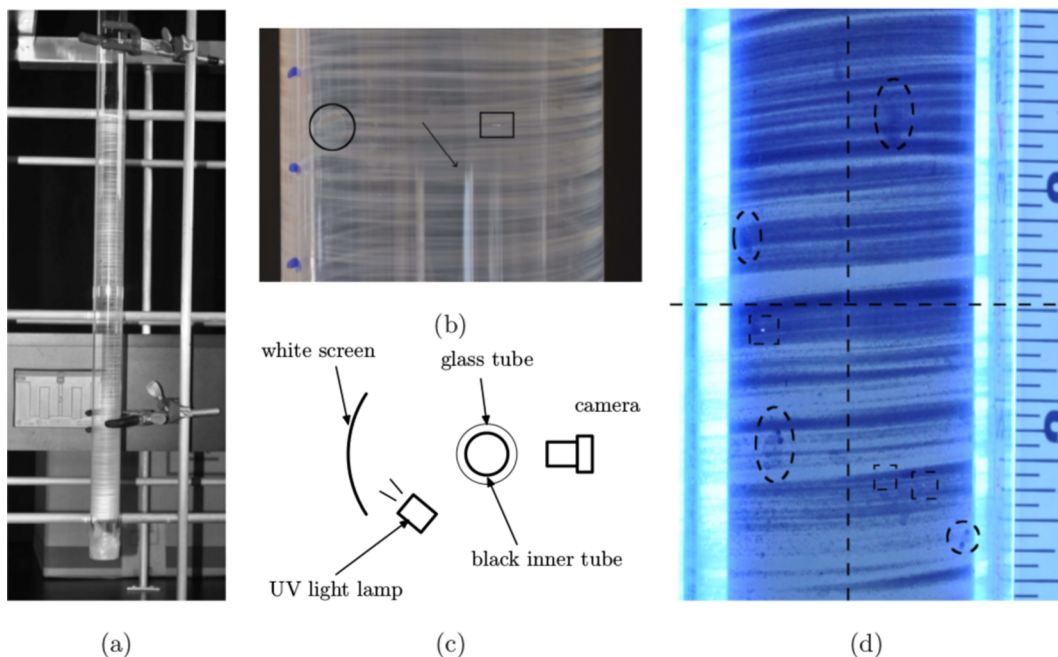


FIG. 1. Experimental setup for the observation of the Liesegang-type pattern phenomenon. (a) A typical fraction of the Liesegang-type pattern generated after several hours. (b) Zoom of the precipitation bands deposited on the wall of a glass tube. Regions of low contrast or, respectively, interference of rear and frontal patterns are visible. (c) Schematic diagram of the setup implemented to improve the photos of the Liesegang-type patterns and (d) typical photo taken with the setup shown in (c). The superposition of frontal and rear patterns is now avoided, the contrast improved and light reflection considerably diminished. Some impairments are marked in (b) and (d): White stripes caused by light reflection pinpointed by arrows, some light dispersion caused by small but macroscopic particles (bright spots) highlighted by rectangles and water marks emphasized by ellipses. The vertical and horizontal dashed lines indicate the cross section of the intensity profile shown in Figure 2.

contact with the tube walls. Then, the whole cloud moves and the bell-shaped structure re-establishes contact with the wall a bit further along the tube, hence forming the next band. In summary, the observed precipitation pattern is the result of a precisely tuned multi-factor reaction-diffusion-convection system, where temperature and concentration gradients are driving forces for the complex dynamics of the reaction cloud. A detailed study of the propagation front and cloud dynamics can be found in Ref. 33.

In order to perform a quantitative analysis of the pattern, a digitalized record of the physical Liesegang bands is required. This is realized by a sequence of photos taken of the glass tube after the experiment has finished. For this purpose a Nikon D5000 digital camera has been mounted on a track parallel to the glass tube in order to (a) keep the distance to the tube constant and (b) to control the lateral shift of the camera for taking the subsequent picture. A photo of a small section of the resulting pattern is shown in Figure 1(b). The spatial structure appears irregular, noise contaminated and the bands are neither strictly parallel nor aligned horizontally. Furthermore, water drops, light reflection, and the deposition of small particles hamper the pattern analysis (see Figs. 1(b) and 1(d)). These adverse effects render the precise localization of a band maximum a difficult task. Well-defined quantitative criteria are necessary for identifying band position and intensity. Some of these impairments can be avoided or at least diminished. For instance, a black tube is placed inside the glass tube after the experiment has finished, which inhibits the interference of the rear face of the tube and simultaneously improves the contrast of the images.

III. IMAGE PROCESSING

In order to reduce light reflection the photos are taken in a dark room and direct illumination of the object is avoided. To achieve this, a white screen is placed behind the tube, which in turn is illuminated by a UV-lamp (see Fig. 1(c)). The illumination is now indirect from the screen to the back side of the tube. This configuration bears the additional advantage of an extended light source that illuminates nearly homogeneously a large portion of the back side. Consequently, the light enters the rear side of the tube and spreads around its circumference, while executing multiple refractions within the disordered precipitation of the salt. Therefore, areas with a larger amount of precipitation, i.e., the Liesegang-type bands, disperse more light and, hence, are shining with a higher intensity. In this way, the precipitation pattern is clearly visible with minimal reflection at the glass surface and the contrast of the photos improves notably, although the contours of water drops become more visible and also the brilliance of small particles on the wall increases (compare Figs. 1(b) and 1(d)). We considered this experimental setup adequate and proceeded with the quantitative data pre-processing.

At first, a sequence of digital photos was taken along the glass tube. The digital photography is a two-dimensional matrix of 4288×2848 pixels, where each pixel is characterized by three variables corresponding to the three fundamental colors (blue, red and green). Each of these variables contain an integer value according to the intensity of the corresponding color ranging from 0 to 255. Thus the intensity I for every color is a function of x, y , where x and

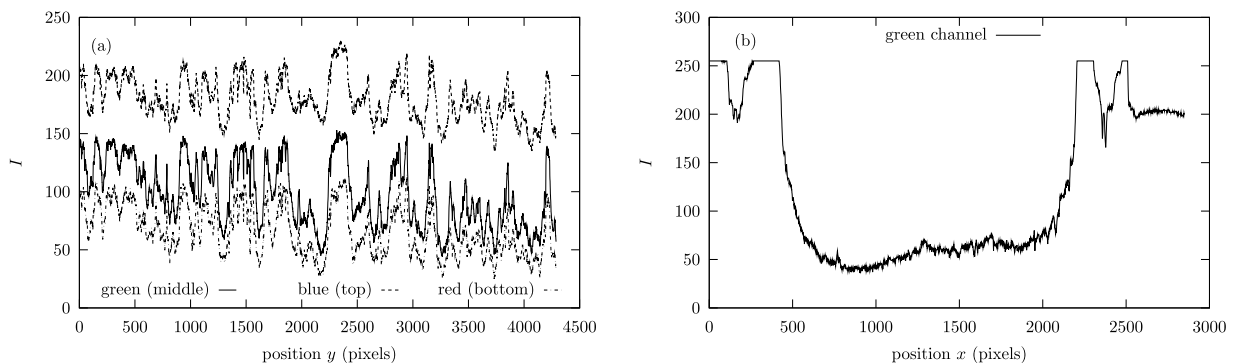


FIG. 2. (a) Intensity $I(x_c, y)$ along the column x_c of the color matrix corresponding to the symmetry axis of the glass tube, which is indicated by the vertical dashed line in the Fig. 1(d). (b) Intensity values of the green color $I(x, y_c)$ along the row $y_c = 2144$ of the color matrix, corresponding to the horizontal dashed line shown in the Fig. 1(d).

y denote columns and rows of the color matrix, respectively. In Figure 2(a) the intensity $I(x_c, y)$ for each color is shown as a function of y , where x is taken as a fixed parameter ($x = x_c$). The chosen longitudinal cut (at position $x_c = 1300$) is indicated as a dashed line in Figure 1(d). The broad intense maximum is easily identified in Fig. 1(d) as a broad peak at about $y \approx 2400$ pixels. In order to express the distance variables x and y in physical units, we use the equivalence 1 pixel = 0.00154 cm, which is derived via a ruler placed on the side the glass tube while taking the photographs. For the purpose of clarity in the image processing, we will keep the more appropriate pixel unit when we refer to distances, meanwhile the final intensity profile will be given as a function of the distance expressed in centimeters.

The curve corresponding to the blue color shows largest intensity values, as it should be expected when using a UV-lamp for illumination. The intensity of the green color shows the highest contrast, i.e., this curve shows the largest variance with best pronounced maxima and minima. For this reason this color was chosen for further data pre-processing. The intensity curves appear to be strongly noise contaminated, partly because of water drops or particle deposition and also due to a high inherent stochastic component of the spatio-temporal evolution of the chemical reaction reflected by the sequence of Liesegang-type bands.

In Figure 2(b) we show the intensity of the green color $I(x, y_c)$ along the horizontal dashed line of Figure 1(d). The maximal intensity at the left and right border (below pixel 500 and above pixel 2000) is caused by the light emitted directly from the screen, passing aside the black inner tube. The region between $x \approx 700$ and 1900 pixels corresponds to the precipitation pattern illuminated by light diffraction.

In order to reduce the considerable amount of noise in the intensity curves, we tried filtering in the Fourier domain. However, this did not establish objective criteria for setting filter parameters like the borders of an appropriate band or low pass filter. On the other hand, if the noise component is spatially uncorrelated, an average over different longitudinal cuts, i.e., cuts parallel to the tube axis, should provide satisfactory results. However, as the precipitation bands are not aligned precisely in the horizontal direction, such an average cannot be taken simply by just summing up the intensity values along transversal or horizontal cuts.

Instead, one has to take into account that the bands are inclined in order to avoid mixing band and gap regions.

For this purpose we applied the cross correlation function between a reference intensity curve $I(x_1, y)$ and every intensity curve $I(x_i, y)$ within the range 800–1800 pixels in Figure 1(b) in order to implement a procedure that allows us to align the inclined bands and thus properly sum up over the transversal cuts. Such procedure is described in the Appendix and its outcome is shown in Figure 3(a), where the photo shown in Figure 1(d) has now the precipitation bands aligned. The one-dimensional average profile $\tilde{I}(y)$ can now be simply taken as an average over the shifted intensity curves $\tilde{I}(x_i, y)$

$$\tilde{I}(y) = \frac{1}{1000} \sum_{i=800}^{1800} \tilde{I}(x_i, y). \quad (1)$$

Notice that about 700–800 pixels from each border of the tube are excluded from the above procedure in order to avoid major distortions due to parallax effects. For a given

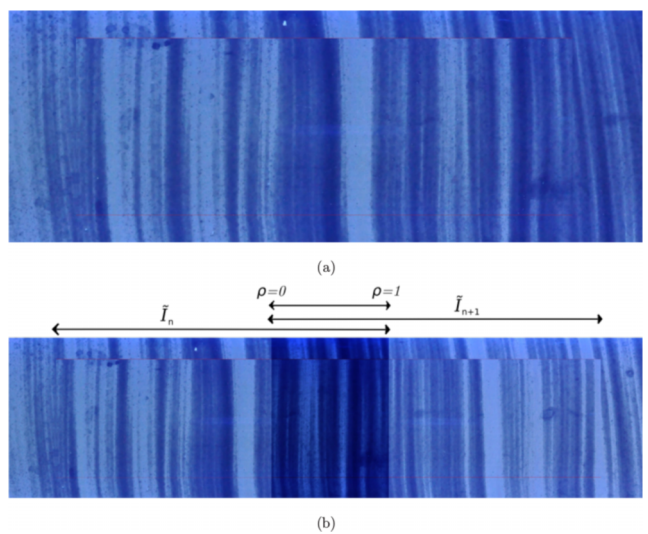


FIG. 3. (a) Processed image corresponding to the photo shown in Figure 1(d), where the precipitation bands are aligned by following the algorithm explained in the Appendix. A section of 700 pixels thick close to the borders of the tube has not been taken into account in the algorithm in order to avoid parallax error. (b) Two photographs merged into a single picture following the recipe drawn in the text. Note that the overlap area was artificially darkened for illustrative purposes only.

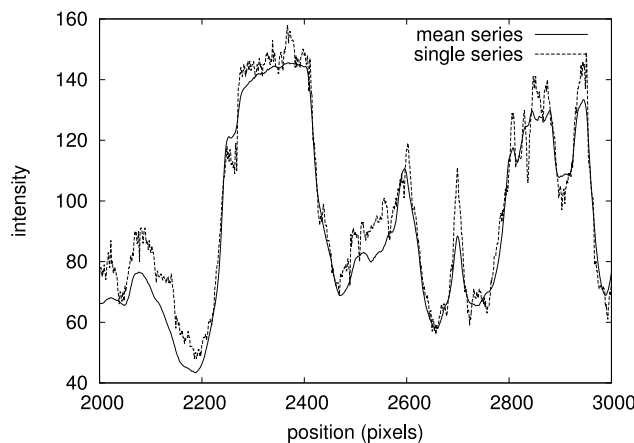


FIG. 4. Comparison between a single intensity curve corresponding to a longitudinal cut along the axis of the tube at $x_c = 1300$ and the average over 1000 aligned intensity curves.

photo, the central part of the tube, which is located just in front of the camera, is most precisely reproduced and the influence of the cylindrical shape of the tube is reduced. Due to its shape the upper and lower border of a photo is deformed, an effect which would induce systematic errors to the averaging process. A comparison of a single intensity curve $I(x_c, y)$ for $x_c = 1300$ and the average $\tilde{I}(y)$ is shown in Figure 4. The considerable reduction of noisy fluctuations of the one-dimensional intensity profile becomes evident. Now, an automated search for the positions of maxima will be much more reliable, since it will not be contaminated by noisy fluctuations which superimpose the band structure of a single cut.

The procedure described so far refers to a single photo corresponding to a small part of the precipitation pattern obtained in the experiment. About 15–17 photos were required to cover the whole band-sequence. In order to obtain a single series for the whole pattern, we paste the series corresponding to every individual photo. For this purpose the photos are taken with an overlap of one third with the neighboring pictures, i.e., about 1430 pixels at each side. In order to assemble the n th and $(n + 1)$ th photos the intensity profile of the overlap region is estimated by a weighted average of the profiles \tilde{I}_n and \tilde{I}_{n+1} obtained from the two neighboring photos

$$\tilde{I}_{n,n+1}(y) = (1 - \rho(y))\tilde{I}_n(y) + \rho(y)\tilde{I}_{n+1}(y), \quad (2)$$

where $\rho(y)$ is a linear weight function that varies from zero to one while moving within the overlap region of the adjacent image. The scheme of the weighted average and the result of an assembly of two photos is illustrated in Figure 3(b).

The resulting intensity profile of the whole sequence of precipitation bands is shown in Figure 5(a). The chemical reaction started at the right side of the figure, which corresponds to the upper part of the tube. The reaction front moves continuously towards the left.

In Figure 5(b) the power spectra of the average intensity profile and that one of a single longitudinal cut at about $x_c = 1300$ is shown for comparison. The contribution of fast frequency components is essentially reduced by the averaging process, which leads to a notable reduction of the fluctuations

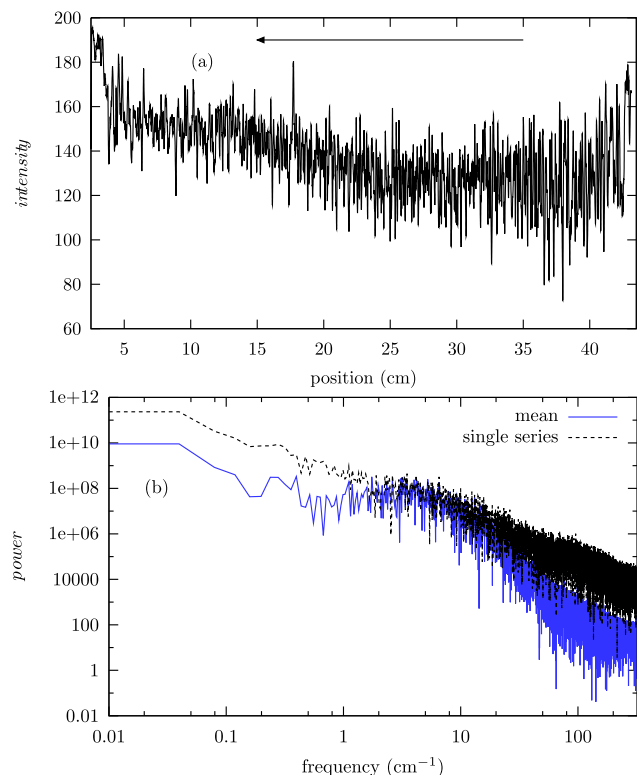


FIG. 5. (a) Intensity profile t_1 extracted from the whole sequence of merged photos of precipitation bands after the image processing as explained in the text. The arrow indicates the direction of the reaction front displacement. (b) Power spectra of the intensity profile shown in (a) (solid line) and a single cut (dashed line).

in the intensity profile (see also Fig. 4). Furthermore, one observes that the power spectrum derived from the average curve is notably reduced over almost the whole frequency range, a clear signature that uncorrelated components are present for all frequencies. This might be the reason why no objective criteria to fix borders of high or low pass Fourier filters could be established. It seems that averaging over longitudinal cuts of the color matrix is an effective tool for noise reduction.

However, when a single maximum bifurcates in two, systematic errors are induced via the averaging process. The broader the region is chosen for the average, the larger is the probability that such incidences occur. Thus, we made a compromise by including as many intensity curves as necessary in order to assure an effective noise reduction, but as few as possible in order to reduce the incidence of band bifurcation. This compromise can be controlled by the power spectrum of the intensity curves. We successively increase the number of vertical cuts in the averaging process from $N = 600$ to $N = 1000$ and tested changes in the power spectral density for each of the resulting intensity profiles. We did not observe any qualitative change of the power spectra when at least 800 has taken into account. Hence, for the quantitative analysis of the precipitation pattern we fixed the number of profiles to $N = 800$.

The intensity profile shown in Figure 5(a) looks still noisy and non-stationary. A smooth modulation of the curve is superimposed by large and apparently irregular

fluctuations. Each of these sharp local maxima, which may vary drastically in intensity and width, correspond to a specific precipitation band. On the other hand, the smooth modulation might be caused by a nonstationary component of the chemical reaction and the dynamics of the reaction cloud. Furthermore, the mean amplitude of the fluctuations decreases systematically during the experiment, i.e., toward the left side of the curve in Fig. 5(a). Both, the smooth modulation as well as the systematic reduction of the variance of the curve might be caused by nonstationary experimental conditions like slow temperature modulation during the experiment or by the continuous consumption of the two reactants.

IV. LOCALIZATION OF BANDS: TEST OF THE SPACING LAW

An immediate and natural analysis of the averaged intensity profile is testing the spacing law $y_{n+1} = p y_n$.⁹ Thus, in this section we proceed to analyze the maxima of the intensity profiles, which requires noise free data series. Although the noise level of the intensity profile could be considerably reduced via the averaging process, a remaining amount of noise contamination is still apparent. Surprisingly, when we do an undiscriminated search for maxima and interpret them as band positions, we get a tendency that it is in agreement with the spacing law $y_{n+1} = p y_n$ ⁹ (see Figure 6(a), where subsequent maxima y_{n+1} vs y_n are

plotted). Furthermore the estimated value for the parameter p corresponds to a reverse Liesegang type pattern as reported in Ref. 18. Similar results were obtained for the remaining tubes.

However, the indiscriminate interpretation of the maxima as genuine precipitation bands may lead to erroneous results when noise is present. We eliminate spurious bands by imposing a minimal number of pixels d_m between consecutive maxima in the algorithm of maxima localization. Then we calculate the nearest-neighbor spacing distribution of bands $P_{nn}(s)$, where s is the spacing between two consecutive bands.

In Figure 6(b) we show the estimated $P_{nn}(s)$ when an undiscriminated search of maxima is done, i.e., when we set $d_m = 2$. The x -axis is normalized by the mean spacing of bands \bar{s} . Notice the prominent peak for small values of s . This is indicative of many consecutive maxima separated by a small distance, as it occurs with the maxima of a noisy signal. Increasing values of the minimal distance d_m should affect sensitively the detection of spurious bands as well as the spacing distribution $P_{nn}(s)$ in the regime of small values of s . In Figure 6(b) we also show the nearest neighbor spacing distribution of bands $P_{nn}(s)$ corresponding to maxima found by imposing a minimal distance $d_m = 4$ pixels between consecutive maxima. Notice the qualitative change in $P_{nn}(s)$, in the regime of small values of s the peak mentioned above is considerably reduced, which indicates that the effect of spurious bands is effectively diminished by increasing d_m . Interestingly, also the overall shape of $P_{nn}(s)$ for large distances is modified.

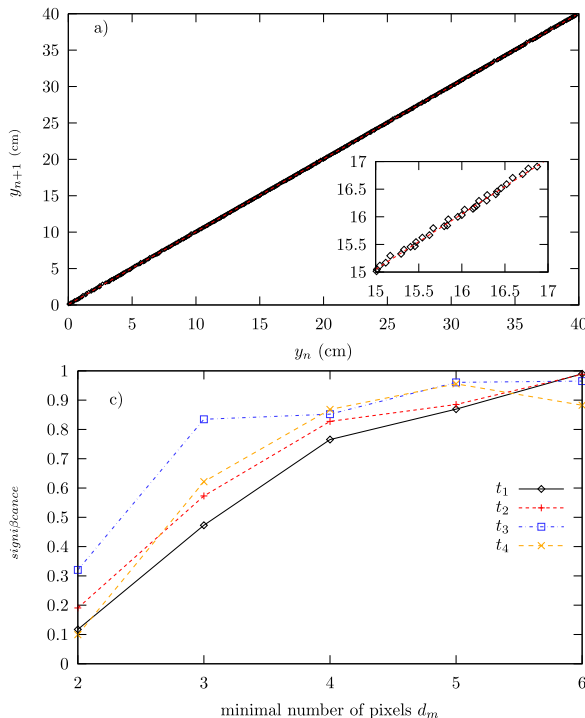
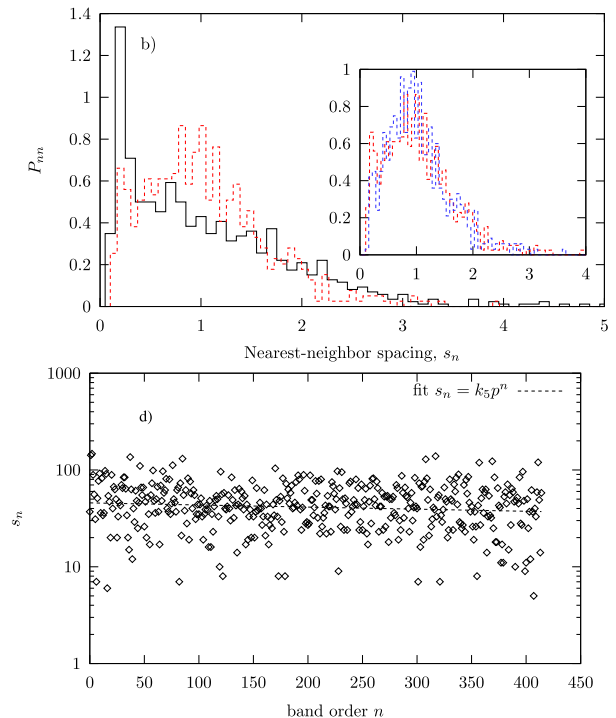


FIG. 6. (a) Test of the spacing law $y_{n+1} = p y_n$ for the series t_1 . The fit of a line (red dashed line) according to the spacing law yields a value for the kinetic coefficient p of $0.9994 \pm 5 \times 10^{-6}$. The value $p < 1$ indicates a reverse Liesegang-type pattern. Notice that only by a zoom is the fitted dashed line distinguishable from the empirical data. (b) Nearest-neighbor spacing distribution of bands $P_{nn}(s)$, for the maxima of t_1 series. A minimal distance of $d_m = 2$ (black solid line) and 4 (red dashed line) pixels between consecutive maxima is imposed in their localization algorithm. The nearest-neighbor spacing s is normalized to the mean spacing \bar{s} . Inset: Corresponding results for $d_m = 4$ and 5 (blue dashed line) show similar behavior. (c) Calculated significance using a Mean-Whitney-Wilcoxon test, for consecutive distributions corresponding to d_m and d_{m+1} , as a function of d_m . Results for the series t_1-t_4 are shown. (d) Nearest-neighbor spacing $s_n = y_{n+1} - y_n$ as a function of the band order n for the maxima of series t_1 . The fit $s_n = k_5 p^n$ according to the spacing law is shown. Again, the nearest-neighbor spacing s is normalized to the mean spacing \bar{s} .



If we further increase the minimal distance d_m we will get rid of spurious bands, however we also increase the probability of the exclusion of genuine structures. Thus, a critical value d_m^c , for which the effect of spurious bands is diminished, can be obtained by increasing d_m until the corresponding distribution $P_{nn}(s)$ remain unchanged. In the inset of Figure 6(b) we show the corresponding distributions for the cases of $d_m = 4$ and 5 pixels, respectively, where the differences are less evident. A quantitative determination of d_m^c is accomplished by a comparison between the distributions $P_{nn}(s)$ obtained for increasing values of d_m using a Mean-Whitney-Wilcoxon test. Figure 6(c) shows the significance calculated for consecutive distributions corresponding to d_m and d_{m+1} . A value of the significance close to unity implies that the two distributions are statistically equivalent. We also show the corresponding results for the series $t_2 - t_4$, where values of 4 and 5 pixels for d_m^c are obtained. Thus, $d_m^c = 5$ pixels seems to be an adequate choice. In this case, the calculated mean spacing of bands \bar{s} for t_1 series is 0.072 cm. Furthermore, it is easy to show that according to the spacing law, the nearest-neighbor spacing $s_n = y_{n+1} - y_n$ obeys the equation $s_n = kp^n$, where k is a constant. In Figure 6(d) we show the nearest-neighbor spacing s_n as a function of the band order n . The fit $s_n = k_5 p^n$ according to the spacing law is also shown. Although the experimental results present large fluctuations, the mean trend is dictated by the spacing law, which indicates the persistence of this aspect of the band structure determined in common Liesegang experiments.

V. SUMMARY AND CONCLUSIONS

In this work we presented the experimental setup, image processing, and noise reduction procedure implemented to obtain a one-dimensional intensity profile of Liesegang-type bands. We like to emphasize that the whole procedure is data driven, i.e., all parameters and partly also methodological details are not imposed but fixed by criteria derived from the characteristics of the data itself. To improve the quality of the photos the glass tube is illuminated in an indirect way such that the light sheds on the tube from behind and is conducted along the circular wall where it eventually leaves the tube. This procedure bears several advantages. At first, light reflections from a direct illumination are avoided. Second, the white screen acts like an extended light source such that a large fraction of the tube is almost homogeneously illuminated. Finally, the light executes multiple refractions within the disordered salt precipitate so that regions with higher salt deposition radiate with higher intensity. Therefore, the brightness on the photos is a direct measure for the amount of salt precipitate at a given position. However, the intensity profiles extracted from the photos are highly noise contaminated. Due to the lack of objective criteria for fixing filter parameters, longitudinal cuts of the color matrix are first shifted such that zero-lag correlations are maximized before averaging. In this way the noisy component of the intensity profile could be considerably reduced. By a weighted average the intensity profiles extracted from different sections of the tube could be merged together, so that an overall single intensity function is obtained that can be used for a

subsequent quantitative analysis. Finally, a single intensity profile for each tube with a drastically reduced noise level could be extracted, which allowed us to perform a test of the spacing law with surprising positive results. Given the apparently turbulent dynamics of the reaction cloud, which is a condition considerably different from the one usually encountered in common Liesegang experiments, this result could not be anticipated.

This research is geared in a substantial part to the acquisition of data for which statistical measures developed in Paper II³² can be applied, namely, random matrix theory^{26–29} and detrended fluctuation analysis,^{30,31} in order to detect and characterize scaling regimes and short and long-range correlations.

ACKNOWLEDGMENTS

This work was supported by CONACyT Mexico (Project No. 156667). J.T.-G. acknowledges financial support via the Grant No. CB-2010/156667.

APPENDIX: PHOTOGRAPH ALIGNMENT PROCEDURE

In this appendix we describe the algorithm developed in order to align the bands within a photo. For this purpose we calculate the cross correlation as a function of the delay τ

$$C(\tau) = \int_{-\infty}^{\infty} I(x_1, y)I(x_2, y + \tau)dy, \quad (A1)$$

between the intensity curve $I(x_1, y)$ located at $x_1 = 1800$ pixels and the previous 1000 longitudinal cuts, i.e., the range between 800 and 1800 in Figure 1(b). As an example we show in Figure 7(a) three correlation functions for $x_2 = x_1 - 5$, $x_1 - 500$, and $x_1 - 1000$, respectively. Over the whole range of x_2 values the maximum of the correlation function remains considerably high with $C_{\max} > 0.7$, which demonstrates the high similarity among the intensity curves in spite of the considerable noise contamination. Hence the dominant structure is neither the noisy background nor systematic impurities like water drops, but more likely the genuine band structure. Furthermore, the larger the spatial distance between two vertical cuts, the larger is the lag where the correlation function encounters its maximum. In fact, the lag of maximal correlation increases almost linearly with the spatial distance between two intensity curves (Figure 7(b)).

Thus, the high correlation between the intensity profiles justifies the averaging over the central part of the photos like that shown in Figure 1(d). Indeed, the relationship between spatial distance and the lag of maximal correlation indicates how to take such average. In fact one has to shift each curve $I(x_2, y)$ relative to $I(x_1, y)$ by the lag of maximal correlation. Thereafter, all curves have maximum zero-lag correlation with the longitudinal cut $I(x_1, y)$ at position $x_1 = 1800$. The result of this procedure is shown in Figure 3(a), which is the equivalent to Figure 1(d), solely the central 1000 vertical cuts are aligned to maximal zero-lag correlations. One observes that now the precipitation bands are almost parallel and horizontally orientated. The spatial average can now be taken as $\tilde{I}(y) = \frac{1}{N} \sum_{i=1}^N \tilde{I}(i, y)$, where the shifted intensity curve

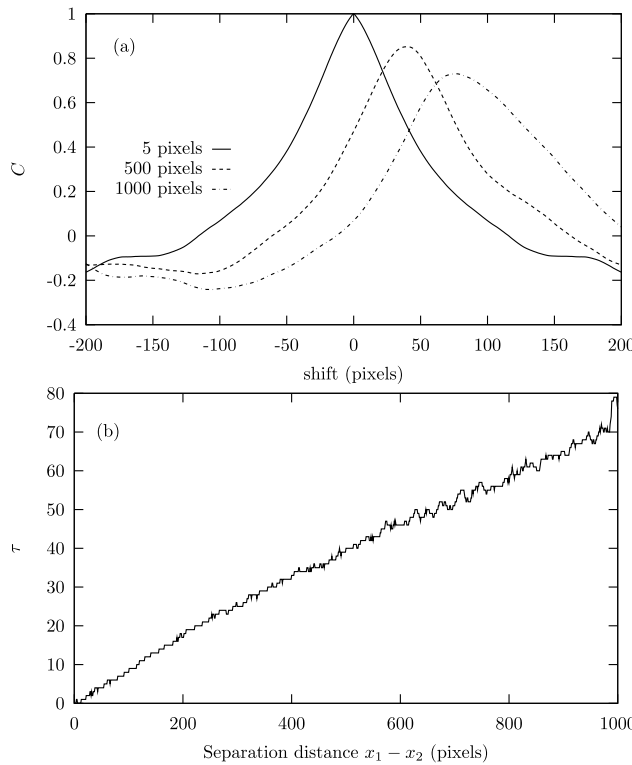


FIG. 7. (a) Cross correlation function between the intensity curve at $x_1 = 1800$ and $x_2 = x_1 - 5$, $x_2 = x_1 - 500$ and $x_2 = x_1 - 1000$, respectively, as a function of the delay, i.e., a relative shift between the two curves. (b) Delay τ for maximal cross correlation as a function of the spatial separation between two intensity curves starting from $x_2 = 1800$ pixels to $x_2 = 800$ pixels.

is termed as $\tilde{I}(i, y)$ while $\tilde{I}(y)$ denotes the one-dimensional average profile. Note the top and bottom of the photos (about 700 pixels from each border) are excluded from this procedure in order to avoid major distortions due to parallax effects.

¹R. E. Liesegang, *Naturwiss. Wochenschrift* **11**, 353-362 (1896).

²G. T. Dee, *Phys. Rev. Lett.* **57**, 275 (1986).

³D. A. Smith, *J. Chem. Phys.* **81**, 3102 (1984).

- ⁴G. Venzi and J. Ross, *J. Chem. Phys.* **77**, 1308 (1982).
- ⁵R. Sultan hompson and P. D. Shipman, *Acta Mech. Sin.* **27**, 119 (2011).
- ⁶A. Toramaru, T. Harada, and T. Okamura, “Experimental pattern in a Liesegang system,” *Physica D* **183**, 133-140 (2003).
- ⁷S. Kai, S. C. Müller, and J. Ross, *J. Phys. Chem.* **87**, 806 (1983).
- ⁸H. W. Morse and G. W. Pierce, *Proc. Am. Acad. Arts Sci.* **38**, 625-647 (1903).
- ⁹K. Jabłczynski, *Bull. Soc. Chim. Fr.* **33**, 1592 (1923).
- ¹⁰S. C. Müller, S. Kai, and J. Ross, *J. Phys. Chem.* **86**, 4078 (1982).
- ¹¹R. Matalon and A. Packter, *J. Colloid Sci.* **10**, 46 (1955); A. Packter, *Kolloid Z.* **142**, 109 (1955).
- ¹²H. K. Henisch, *Periodic Precipitation* (Pergamon Press, 1991).
- ¹³A. Büki, É. Kárpáti-Smidróczki, and M. Zrínyi, *Physica A* **220**, 357 (1995).
- ¹⁴T. Antal, M. Droz, J. Magnin, and Z. Racz, *Phys. Rev. Lett.* **83**, 2880 (1999); Z. Racz, *Physica A* **274**, 50-59 (1999).
- ¹⁵B. Chopard, P. Luthi, and M. Droz, *J. Stat. Phys.* **76**, 661 (1994).
- ¹⁶S. Chen and G. D. Doolen, “Lattice Boltzmann method for fluid flows,” *Annu. Rev. Fluid Mech.* **30**, 329 (1998).
- ¹⁷T. Antal, M. Droz, J. Magnin, Z. Racz, and M. Zrínyi, *J. Chem. Phys.* **109**, 9479 (1998).
- ¹⁸M. Flicker and J. Ross, *J. Chem. Phys.* **60**, 3458 (1974).
- ¹⁹G. Varghese and M. A. Ittyachen, *J. Mater. Sci. Lett.* **11**, 916 (1992); G. Varghese, M. A. Ittyachen, and C. Joseph, *J. Mater. Sci.* **28**, 6357 (1993).
- ²⁰M. Attieh, Al-Kassem, and R. Sultan, *J. Chem. Soc., Faraday Trans.* **94**, 2187 (1998).
- ²¹E. L. Spotz and J. O. Hirschfelder, *J. Chem. Phys.* **19**, 1215 (1951).
- ²²M. A. Einarsrud, F. A. Maao, A. Hansen, M. Kirkedelen, and J. Samseth, *Phys. Rev. E* **57**, 6767 (1998).
- ²³P. Kasten and M. Kahlweit, *Ber. Bunsenges. Phys. Chem.* **74**(6), 546-551 (1970).
- ²⁴S. Thompson and P. D. Shipman, *Proc. IUTAM* **9**, 138 (2013).
- ²⁵G. A. Davies, A. B. Ponter, and S. Singh, *Nature* **213**, 279 (1967).
- ²⁶E. P. Wigner, *Ann. Math.* **53**, 36 (1951); *Proc. Cambridge Philos. Soc.* **47**, 790 (1951).
- ²⁷M. L. Mehta, *Random Matrices* (Academic Press, London, 1990).
- ²⁸T. A. Brody, J. Flores, J. B. French, P. A. Mello, A. Pandey, and S. S. M. Wong, *Rev. Mod. Phys.* **53**, 385 (1981).
- ²⁹T. Guhr, A. Müller-Groeling, and H. A. Weidenmüller, *Phys. Rep.* **299**, 189 (1998).
- ³⁰K. Hu, P. Ch. Ivanov, Z. Chen, P. Carpena, and H. E. Stanley, *Phys. Rev. E* **64**, 011114 (2001).
- ³¹J. W. Kantelhardt, E. Koscielny-Bunde, H. H. A. Rego, S. Havlin, and A. Bunde, *Physica A* **295**, 441 (2001).
- ³²J. C. Torres-Guzmán, G. Martínez-Mekler, and M. F. Müller, *J. Chem. Phys.* **144**, 174702 (2016).
- ³³E. Ramírez-Álvarez *et al.*, “On the dynamics of Liesegang-type pattern formation in a gaseous system,” *Sci. Rep.* **6**, 23402 (2016).